
Spatial Variation of Resolution and Noise in Multi-Detector Row Spiral CT¹

John F. Meinel, Jr, BSE, Ge Wang, PhD, Ming Jiang, PhD, Troy Frei, Michael Vannier, MD, Eric Hoffman, PhD

Rationale and Objectives. The authors performed this study to evaluate an approach for measuring the variations of three-dimensional spatial resolution and image noise throughout a field of view imaged with multi-detector row spiral computed tomographic (CT) scanners.

Materials and Methods. The authors designed a phantom (diameter, 320 mm) that contained 37 metallic spheres (diameter, approximately 0.8 mm) positioned between two disks made of a material with attenuation being that of water. One sphere was located at the isocenter of the phantom, and the rest were evenly spaced in three concentric rings with diameters of 100, 200, and 300 mm, respectively. The phantom was imaged with two widely used multi-detector row CT scanners by using a standard protocol and four variations of that protocol. Because a recently developed theory holds that image resolution should be proportional to the square root of the trace of the covariance matrix of a point spread function, the authors developed a software package to segment high-attenuation spheres from the CT image volume and compute point spread functions from blurred images of the spheres. Three-dimensional spatial resolution and image noise were calculated as a function of radial distance within the field of view.

Results. Resolution and noise were quantified in the resultant CT image volumes and found to be nonisotropic, with worse resolution and less noise occurring at the periphery of the field of view.

Conclusion. The method enabled measurement of variations in spatial resolution and of their distribution on images obtained with multi-detector row CT scanners. These findings may contribute to the development of an improved algorithm for image reconstruction.

Key Words. Computed tomography (CT), image quality; computed tomography, multi-detector row; computed tomography (CT), quantitative.

© AUR, 2003

During the past few years, rapid progress has been made in computed tomographic (CT) theory, technology, and applications, and multi-detector row CT has become a standard modality of medical imaging. Objective, quanti-

tative, CT image-based measures are gaining acceptance in the clinical setting as diagnostic aids for characterizing pathologic processes and as predictors of therapeutic outcomes. Image quality is thus of primary concern. Extensive studies of various methods for quantitative and qualitative assessment of CT image quality have produced many valuable results (1–5).

A number of factors contribute to image quality, including the choice of a CT scanner and scanning protocol. In this study, we investigated various parameters that affect spatial resolution and image noise. Previous research studies of image quality were focused mainly on the center of the field of view, and most were concerned

Acad Radiol 2003; 10:607–613

¹ From the Departments of Biomedical Engineering (J.F.M., G.W., E.H.) and Radiology (G.W., T.F., M.V., E.H.), University of Iowa College of Medicine, 200 Hawkins Dr, Iowa City, IA 52242; and the School of Mathematics, Peking University, Beijing, China (M.J.). Supported in part by National Institutes of Health, Bioengineering Research Partnership grants R01-HL-064368 and R01-DC-03590. Received January 21, 2003; revision requested February 6; revision received and accepted February 18. **Address correspondence to G.W.**

© AUR, 2003

with either in-plane resolution (the ability to resolve two objects in a single section) or through-plane resolution (the ability to resolve objects in two different sections). We performed this study to evaluate variations in three-dimensional resolution and noise throughout the field of view on multi-detector row CT images obtained in a disk-shaped phantom containing concentric rings of metallic spheres. We chose to measure noise instead of contrast resolution because the measurement of noise is less complicated than that of contrast resolution. We developed a simple method for calculating three-dimensional resolution and image noise at multiple points throughout a field of view.

In the next section, we describe a phantom that was created to enable these measurements. Then we discuss how we quantified three-dimensional spatial resolution by using a formula for computing the square root of the trace of the covariance matrix of a point spread function (6,7). We also discuss briefly how we measured image noise. Finally, we present our results, discuss the possible origins of the observed variations in resolution, and suggest possible directions of future research.

MATERIALS AND METHODS

Phantom

To study how spatial resolution varies within the field of view of a reconstructed CT scan, we created a phantom that enabled us to measure spatial resolution at multiple points. With the commonly used line-pair phantoms or wire phantoms, resolution can be measured in only one or two dimensions; because we wanted to measure spatial resolution in all three dimensions simultaneously, we needed a structure that was more substantially three-dimensional.

It was determined that metal spheres of sufficiently small diameter would provide a reasonable approximation of a delta function in all three dimensions (8). In addition, the shape of the spheres would make it possible to compensate for their finite size. Because spheres are isometric, any misalignment of the phantom with the scanner would have a minimal effect on measurement.

The phantom was disk shaped (ie, a short cylinder) and had a diameter of 320 mm and a height of 20 mm. The spheres were sandwiched between two disks made of a material with attenuation being that of water (height of each disk, 10 mm). The disks were held together with nylon screws. The spheres had a mean diameter (\pm stan-

Table 1
CT Imaging Parameters

Parameter	Scanner	
	Aquilion	MX8000
Kilovoltage	120	120
Milliamperage	300	300
Field of view (mm)	320	320
Collimation (mm)	1	1
Section thickness (full width at half maximum, mm)	1.3	1.3
Number of detector rows	4	4
Pitch	0.625	0.625
Scanning period (sec per revolution)	1	1
Section spacing	0.6	0.6
Scanning path	Helical	Helical
Reconstruction filter	FC01	B
Interpolation method	Full scan	Full scan
Reconstruction matrix	512 × 512	512 × 512
Pixel size (mm)	0.625	0.625
Resolution at isocenter	0.70	0.72

Note.—The FC01 filter used with the Aquilion unit is a standard nonsharpening nonsmoothing filter and is similar to the B filter used with the MX8000 unit.

dard deviation) of 0.79 mm \pm 0.025 (1/32 inch \pm 0.001). One sphere was placed at the isocenter of the phantom, and the others were placed in concentric rings around it, at radii of 50, 100, and 150 mm from the isocenter. Each ring contained 12 equiangularly spaced spheres, for a total of 37 spheres.

Spatial Resolution

An axiomatically sound measure of image resolution in one dimension is the standard deviation of the point spread function (6). This measurement of resolution can be extended to three dimensions by calculating the square root of the trace of the covariance matrix of the point spread function (7). We derived a simple method for computing this measurement that included compensation for convolution with a sphere (Appendix).

Image Noise

The most common measure of noise is the standard deviation of attenuation values in a region that should have uniform value, such as water background. This measure of noise also has an axiomatic basis (6). In our phantom tests, we measured the standard deviation in a region

Table 2
Cross-Protocol Parameters Used with the Phillips MX8000 Scanner

Parameter	Protocol Name			
	High-Resolution Sharp	1,024	Half Scan	0.5 mm
Collimation (mm)	1	1	1	0.5
Section thickness (full width at half maximum)	1.3	1.3	1.3	0.6
Section spacing (mm)	0.6	0.6	0.6	0.6
Focus resolution	High	Standard	Standard	Standard
Interpolation method	Full scan	Full scan	Half scan	Full scan
Reconstruction filter	Sharp	Standard	Standard	Standard
Reconstruction matrix	512 × 512	1,024 × 1,024	512 × 512	512 × 512
Resolution at isocenter	0.72	0.50	0.7	0.56

Note.—Four scans were obtained by using different parameters.

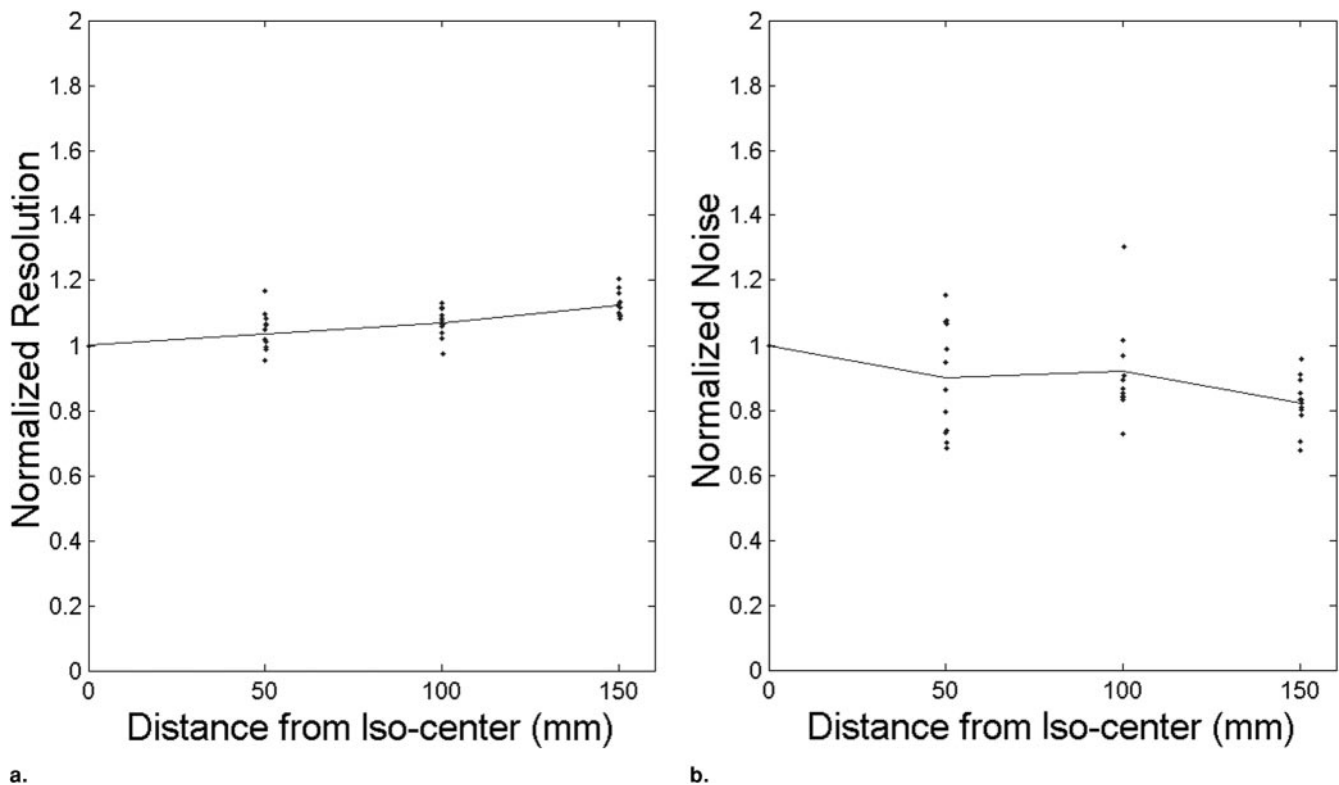


Figure 1. Graphs of variations in (a) spatial resolution and (b) noise correlated with distance from the isocenter on CT images obtained in the disk phantom by using the Aquilion scanner. Each x-axis location represents a ring of spheres inside the phantom. The line connects the mean measurements in each of the three concentric rings. For both resolution and noise, lower numbers are better. Notice that as spatial resolution becomes worse toward the periphery of the field of view, noise also is reduced. Imaging parameters are given in Table 1.

of interest near each of the spheres. This ensured coverage equivalent to that used for measuring spatial resolution.

Scanning Protocols

In the first part of our study, we compared two commercial CT scanners: the Aquilion (Toshiba, Tokyo, Ja-

pan) and the MX8000 (Philips, Cleveland, Ohio). The parameters used at this stage (Table 1) were those of “conventional” scanning; the reconstruction kernel chosen did not enhance or smooth, and the reconstructed voxels were isometric. Scanning parameters were chosen that were as similar as possible between the two imagers.

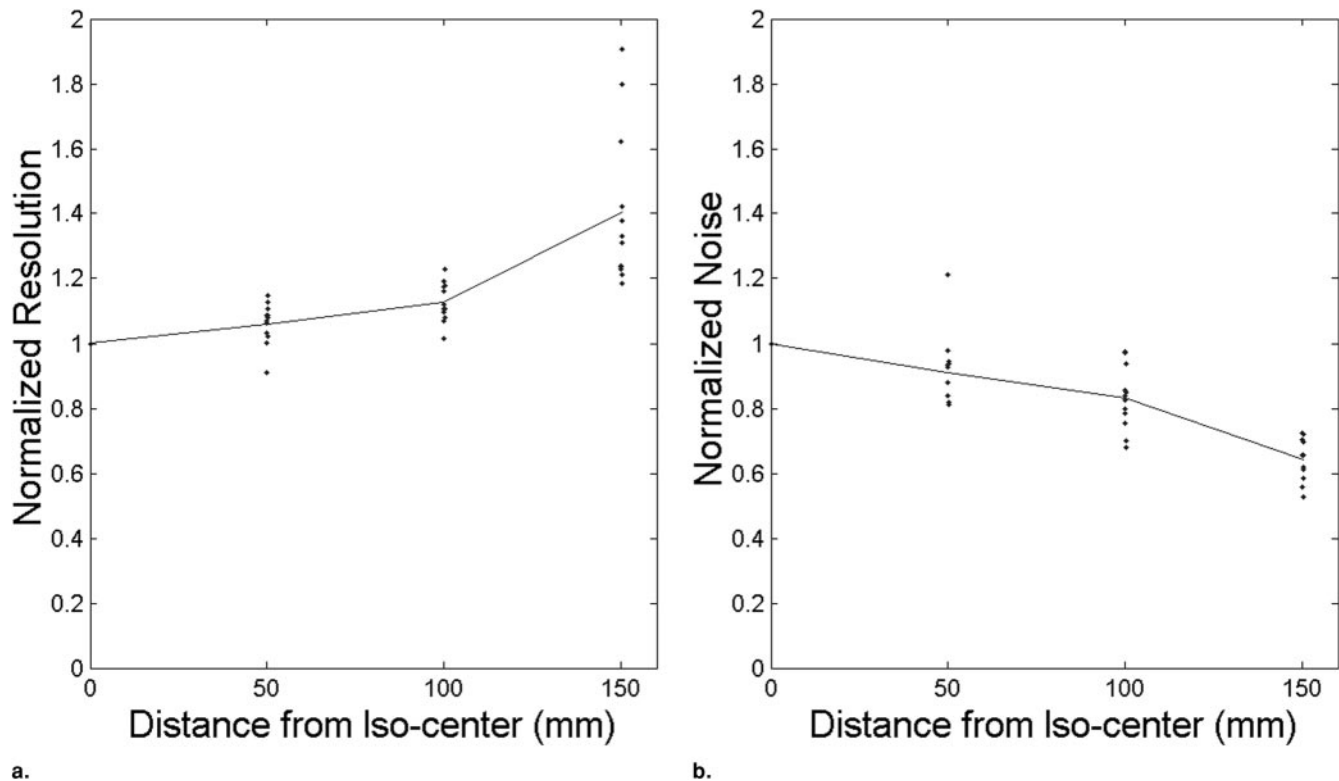


Figure 2. Graphs of variations in (a) spatial resolution and (b) noise correlated with distance from the isocenter on CT images obtained in the disk phantom by using the Philips MX8000 scanner. Each x-axis location represents a ring of spheres inside the phantom. The line connects the mean measurements in each of the three concentric rings. For both resolution and noise, lower numbers are better. Notice that as spatial resolution becomes worse toward the periphery of the field of view, noise also is reduced. Imaging parameters are given in Table 1.

The second part of our study was designed to reveal any effects caused by a particular parameter in the scanning protocol. Additional scans were obtained with the MX8000 unit, each with a different variation in the protocol. Representative permutations are described in Table 2.

RESULTS

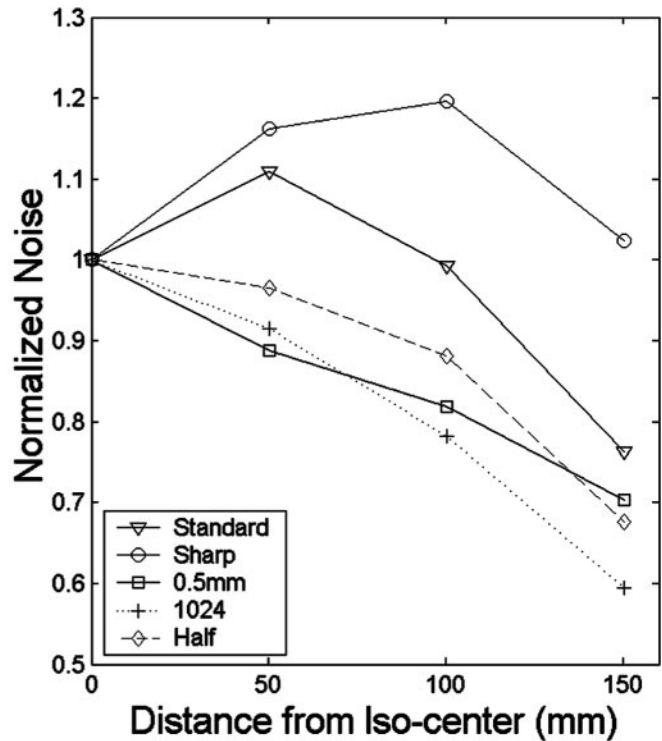
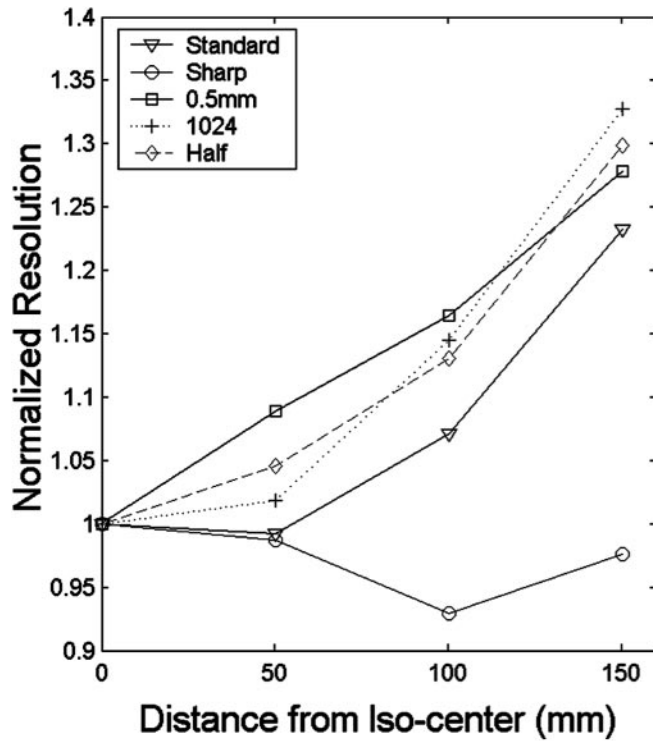
Results from the initial stage of scanning (with the standard protocol) are shown in Figures 1 and 2. Each x-axis location represents a ring of spheres, and the y axis represents normalized resolution or noise. The line connects the mean measurements in each of the three concentric rings of spheres. Spatial resolution varied among spheres within the same ring and became worse with increasing distance from the isocenter (from ring to ring), whereas noise improved with increasing distance from the isocenter.

Images acquired with variations of the standard protocol showed similar results. Figure 3 shows the values ob-

tained with the alternate use of half-scan reconstruction, 0.5-mm collimation, a reconstruction matrix of $1,024 \times 1,024$, and a high-resolution setting with a sharpening filter. Most of these variations in imaging parameters produced results similar to those obtained with the standard parameters. When a sharpening filter was used for reconstruction, however, the variation in resolution was greatly decreased. Figure 4 shows the resolution-to-noise ratio for each of the protocols.

DISCUSSION

Figure 3 shows that resolution and noise are dependent on the distance of the spheres from the isocenter. Spatial resolution decreased as distance from the isocenter increased. The extent of the variation in resolution depends on the scanner and protocol. It may be possible to limit variability in resolution by applying different reconstruction filters, as shown by the values obtained with use of the sharpening filter. The image noise also decreased with



a.

b.

Figure 3. Graphs show (a) the average resolution and (b) average noise at each ring on CT images obtained with the MX8000 by using the standard protocol (Table 1) or one of four variations (Table 2). Notice that the trends are similar, except for the one in which the “sharp” reconstruction kernel was used. ▽ = standard protocol (Table 1), ○ = standard protocol with high-resolution setting and “sharp” reconstruction filter, □ = standard protocol with 0.5-mm section collimation and 0.6-mm section thickness, + = standard protocol with matrix of $1,024 \times 1,024$, ◇ = standard protocol with half-scan interpolation.

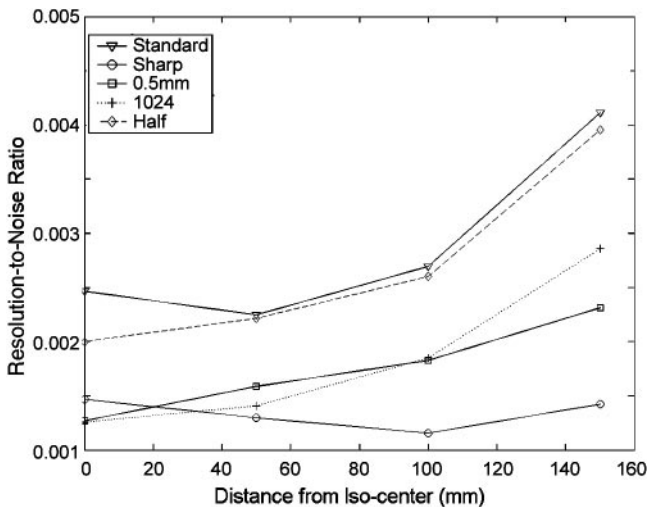


Figure 4. Curves show the average resolution-to-noise ratios on CT images obtained with the standard protocol (Table 1) or with one of four variations (Table 2). The standard protocol provided the best resolution-to-noise ratio throughout the field of view. ▽ = standard protocol (Table 1), ○ = standard protocol with high-resolution setting and “sharp” reconstruction filter, □ = standard protocol with 0.5-mm section collimation and 0.6-mm section thickness, + = standard protocol with matrix of $1,024 \times 1,024$, ◇ = standard protocol with half-scan interpolation.

increasing distance from the isocenter. Once again, however, the use of a sharpening filter muted this effect, causing a notable increase in overall noise.

A scanner that is improperly configured or misaligned with the intended field of view also might cause substantial variation in resolution. If the detector plane is not lined up perfectly with the plane of the x-ray photons, then the detectors at the edge will not receive as many direct x-ray photons as they would with proper alignment. Another common cause of variable resolution is improper collimation. Some have argued that this problem is intrinsic to multi-detector row CT. When multiple detectors are used, a small cone angle results in nonuniform coverage by x-ray photons; that is, a smaller area may be covered on the side nearest the x-ray tube than on the side nearest the detector. This error and its effect on image reconstruction often go unnoticed.

Because numerous factors contribute to image reconstruction, we cannot completely explain why the noise improved away from the isocenter while the spatial reso-

lution became worse. This study was designed to develop and test an axiomatic method for image quality measurement. A more in-depth data analysis may be attempted in future studies.

We could extend this research also by comparing variations in resolution between CT scanners with a single detector row and those with multiple detector rows to determine whether variations correlate with the type of scanner used. The inclusion of a larger selection of multi-detector row scanners would help control for effects unique to manufacturer or model. In addition, it may be valuable to work more directly with the scanner manufacturers in investigating this problem and testing potential solutions. Image reconstruction methods that involve the use of a spatially invariant blurring function may be further improved (9).

Our research also could be extended by testing the approximations made in our computation of three-dimensional resolution. Quantification of how well the isotropic model fits the true point spread function, as well as analysis of the relation between the asymmetry of the point spread function and its location, also might be useful.

In conclusion, we have shown that the spatial resolution of multi-detector row CT reconstruction is better at the center of the field of view and worse at the periphery. Our study of how resolution and noise vary throughout the field of view was made possible by the construction of the phantom and facilitated by the development of a simple method for computing three-dimensional resolution. These tools, and the results they helped us achieve in this study, may be used to guide algorithm development, which in turn may lead to improvements in reconstruction quality.

APPENDIX: COMPUTATION OF AN AXIOMATIC MEASURE FOR IMAGE RESOLUTION

The point spread function p is assumed to have zero mean without loss of generality because we always align our measurement with the center of the point spread function. The resolution measure $R(p)$ of p , up to a constant multiple, is given as

$$R(p) = \sqrt{\text{trace}(\sigma)}$$

$$= \sqrt{\sigma_{1,1}^2 + \sigma_{2,2}^2 + \sigma_{3,3}^2}, \tag{A1}$$

where σ is the covariance matrix of p with elements σ_{ij} , as follows:

$$\sigma_{ij} = \iiint x_i x_j p(\vec{x}) d\vec{x}. \tag{A2}$$

Therefore, the trace of σ is

$$R(p) = \sqrt{\sum_i \sigma_{ii}}$$

$$= \sqrt{\sum_i \iiint x_i^2 p(\vec{x}) d\vec{x}}$$

$$= \sqrt{\sum_i \iiint \|\vec{x}\|^2 p(\vec{x}) d\vec{x}}. \tag{A3}$$

Assume that we have a data volume that contains the point spread function; $v(x, y, z)$ is the value at location x, y, z . If the volume is a perfect point spread function, then $v(x, y, z) = p(x, y, z)$ for each voxel. We define the step size in the $x, y,$ and z directions to be $\Delta x, \Delta y,$ and $\Delta z,$ respectively, and the coordinate origin as the center of the point spread function. Then, to compute the integral (3) numerically,

$$R(p) = \sqrt{\sum_i \iiint \|\vec{x}\|^2 p(\vec{x}) d\vec{x}}$$

$$\approx \sqrt{\sum_{x,y,z} (x^2 + y^2 + z^2) v(x, y, z) \Delta x \Delta y \Delta z}. \tag{A4}$$

Note that we have assumed $x \equiv x_1, y \equiv x_2,$ and $z \equiv x_3,$ for convenience.

For our measurements, we do not have a volume containing a perfect point spread function. We have a volume of a point spread function convolved with a small sphere. To compensate for this, two steps are necessary. First, we need to apply an intensity normalization, as follows:

$$R_{\text{norm}}(p) = \sqrt{\frac{\sum_{x,y,z} (x^2 + y^2 + z^2) v(x, y, z) \Delta x \Delta y \Delta z}{\sum_{x,y,z} v(x, y, z)}}. \tag{A5}$$

$R_{\text{norm}}(p)$ is now a resolution measure of the convolution of the point spread function and a sphere. The variance of a convolution is simply the sum of the component variances or

$$R_{\text{norm}}(p) = \sigma_{\text{sphere}}^2 + \sigma_{\text{PSF}}^2. \quad (\text{A6})$$

To invert the effect of the convolution, we use the following equation:

$$\sigma_{\text{PSF}} = \sqrt{R_{\text{norm}}^2(p) - \sigma_{\text{sphere}}^2}, \quad (\text{A7})$$

which requires a known σ_{sphere} . To calculate the σ_{sphere} , first assume a sphere of uniform distribution with radius r . The sphere is represented as

$$p(\rho, \theta, \phi) = \begin{cases} p_0 = \frac{3}{4\pi r^3} & 0 < \rho < r; \\ 0 & \text{otherwise} \end{cases} \quad (\text{A8})$$

in spherical coordinates with the center of the sphere at the origin.

With use of Equation A3,

$$\sigma_{\text{sphere}}^2 = \iiint \|\vec{x}\|^2 p_0 d\vec{x}. \quad (\text{A9})$$

With use of spherical coordinates,

$$\begin{aligned} x_1 &= \rho \sin(\phi)\cos(\theta) \\ x_2 &= \rho \sin(\phi)\sin(\theta) \quad \text{and} \\ x_3 &= \rho \cos(\phi). \end{aligned} \quad (\text{A10})$$

Therefore, $\|\vec{x}\|^2$ is

$$\begin{aligned} \|\vec{x}\|^2 &= [\rho \sin(\phi)\cos(\theta)]^2 + [\rho \sin(\phi)\sin(\theta)]^2 + [\rho \cos(\phi)]^2 \\ &= \rho^2. \end{aligned} \quad (\text{A11})$$

If we substitute this into Equation A9, we get

$$\begin{aligned} \sigma_{\text{sphere}}^2 &= \iiint \|\vec{x}\|^2 p_0 d\vec{x} \\ &= \int_0^r \int_0^\pi \int_0^{2\pi} p_0 \rho^2 \rho^2 \sin(\phi) d\phi d\theta d\rho \\ &= p_0^{4/5} \pi r^5 \\ &= \frac{3\pi r^2}{5}. \end{aligned} \quad (\text{A12})$$

To study the spatial variation of resolution, we normalize the value at each sphere location ($\sigma_{\text{PSF},i}$) with the value at the isocenter ($\sigma_{\text{PSF},0}$), as follows:

$$\sigma'_{\text{PSF},i} = \frac{\sigma_{\text{PSF},i}}{\sigma_{\text{PSF},0}}.$$

ACKNOWLEDGMENTS

The authors are grateful to Jered Sieren and Osama Saba for scanning the phantom with the Philips MX8000 scanner. They are also grateful to John Dyson and Michael Wardenburg of Medical Instruments, University of Iowa, Iowa City, for the construction of the phantom.

REFERENCES

1. Mahesh M. Search for isotropic resolution in CT from conventional through multiple-row detector. *RadioGraphics* 2002; 22:949–962.
2. Fuchs T, Kachelriess M, Kalender WA. Technical advances in multi-slice spiral CT. *Eur J Radiol* 2000; 36:69–73.
3. Kalender WA, Fuchs TO, Kachelriess M. System performance of multi-slice spiral computed tomography. *IEEE Eng Med Biol* 2000; 19:63–70.
4. Kalender WA, Polacin A, Suss C. A comparison of conventional and spiral CT: an experimental study on the detection of spherical lesions. *J Comput Assist Tomogr* 1994; 18:167–176.
5. Kalender WA, Polacin A. Physical performance characteristics of spiral CT scanning. *Med Phys* 1991; 18:910–915.
6. Wang G, Li Y. Axiomatic approach for quantification of image resolution. *IEEE Signal Processing Lett* 1999; 6:257–258.
7. O'Sullivan JA, Jiang M, Ma XM, Wang G. Axiomatic quantification of multi-dimensional image resolution. *IEEE Signal Processing Lett* 2002; 9:120–122.
8. Kalender WA. Thin-section three-dimensional spiral CT: is isotropic imaging possible? *Radiology* 1995; 197:578–580.
9. Wang G, Vannier M, Skinner MW, Cavalcanti MGP, Harding G. Spiral CT image deblurring for cochlear implantation. *IEEE Trans Med Imaging* 1998; 17:251–262.